JACS
JOURNAL OF THE AMERICAN CHEMICAL SOCIETY
Article
Cite This: J. Am. Chem. Soc. 2019, 141, 11641−11650
pubs.acs.org/JACS

Continuous Partial Oxidation of Methane to Methanol Catalyzed by Diffusion-Paired Copper Dimers in Copper-Exchanged Zeolites

Kimberly T. Dinh,[†,∥] Mark M. Sullivan,[†,∥] Karthik Narsimhan,[†] Pedro Serna,[‡] Randall J. Meyer,[‡] Mircea Dincă,[§] and Yuriy Román-Leshkov*[,†]

[†]Department of Chemical Engineering, Massachusetts Institute of Technology, 77 Massachusetts Avenue, Cambridge, Massachusetts 02139, United States

[‡]ExxonMobil Research and Engineering, Annandale, New Jersey 08801, United States

[§]Department of Chemistry, Massachusetts Institute of Technology, 77 Massachusetts Avenue, Cambridge, Massachusetts 02139, United States

Supporting Information

ABSTRACT: Copper-exchanged zeolites can continuously and selectively catalyze the partial oxidation of methane to methanol using only oxygen and water at low temperatures, but the genesis and nature of the active sites are currently unknown. Herein, we demonstrate that this reaction is catalyzed by a $[Cu-O-Cu]^{2+}$ motif that forms via a hypothesized proton-aided diffusion of hydrated Cu ions within the cages of SSZ-13 zeolites. While various Cu configurations may be present and active for methane oxidation, a dimeric Cu motif is the primary active site for selective partial methane oxidation. Mechanistically, CH_4 activation proceeds via rate-determining C−H scission to form a surface-bound C_1 intermediate that can either be desorbed as methanol in the presence of H_2O/H^+ or completely oxidized to CO_2 by gas-phase O_2. High partial oxidation selectivity can be obtained with (i) high methane and water partial pressures and (ii) maximizing Cu dimer formation by using zeolites with high Al content and low Cu loadings.

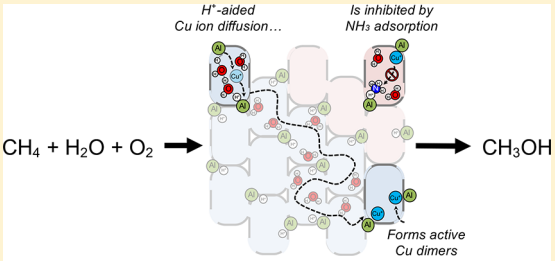

[Cu-O-Cu]²⁺-catalyzes CH_4 partial oxidation in Cu-SSZ-13

INTRODUCTION

The selective oxidation of CH_4 to value-added chemicals remains a grand challenge in catalysis.[1−3] Current industrial processes to upgrade CH_4 to petrochemical precursors require high temperatures (>1000 K) and pressures (>40 bar) and are only economical at large scales,[4] but the increasing availability of natural gas in remote locations necessitates the development of smaller scale CH_4 conversion processes under mild conditions.[5] Iron[6] and copper[7,8] metalloenzymes selectively convert CH_4 to methanol directly at ambient conditions, but these enzymes suffer from limited temperature stability for industrial operation.[9,10] Similar to biological systems, small metal clusters and single metal atoms (Fe,[6,11,12] Cu,[13−20] Rh,[21] Pd[22]) within zeolites are capable of converting CH_4 to methanol at mild conditions. Of particular interest are Cu-exchanged zeolites that activate CH_4 using molecular oxygen as the sole oxidant.[13,18,23−27] Although highly selective, nearly all reported oxidation processes using Cu-exchanged zeolites operate in a cyclic, stoichiometric manner, requiring an anhydrous catalyst reactivation step at high temperatures.

A standout report in this context is the recent work by Narsimhan et al., who demonstrated the first instance of a continuous, gas phase catalytic process for the direct conversion of CH_4 to methanol.[28] The system used Cu-exchanged zeolites to produce methanol using exclusively CH_4, H_2O, and O_2 at 473 K. This process featured high selectivity across a wide range of zeolite topologies, albeit at very low conversion (0.001%). Although catalytic processes offer significant advantages over thermochemical cycling processes, continuous methanol production systems remain largely unexplored,[29] and practical applications necessitate fundamental understanding for catalyst and process improvement.[30] Primarily, the nature and genesis of the active sites involved in catalytic C−H activation are currently unknown.[31] While similarities between the stoichiometric and catalytic systems may exist, it is uncertain if the well-characterized active sites of stoichiometric oxidation systems[20,24,32,33] are related to those active in a catalytic process. In fact, the notable differences between the activity and water tolerance of the active sites in Cu-exchanged zeolites under stoichiometric versus catalytic oxidation reaction conditions[30] suggest that the active sites for the two processes may be entirely different from each other. This work, for the first time, details the kinetics and active site of Cu-exchanged zeolites for the continuous catalytic partial oxidation of methane to methanol using dioxygen in the presence of water.

Received: May 7, 2019
Published: June 21, 2019

DOI: 10.1021/jacs.9b04906
J. Am. Chem. Soc. 2019, 141, 11641−11650

Table 1. Composition and Synthesis Method for SSZ-13 Zeolites[a]

catalyst	composition			Cu content (wt %)	Cu/cage	synthesis method
	Si/Al	Cu/Al	Na/Al			
H−CHA	8.8					2−6MR[b]
Cu−CHA(0.05)	8.8	0.04		0.41	0.05	2−6MR, Cu-IE[c]
Cu−CHA(0.10)	8.8	0.08		0.76	0.10	2−6MR, Cu-IE
Cu−CHA(0.12)	8.8	0.10		0.90	0.12	2−6MR, Cu-IE
Cu−CHA(0.20)	8.8	0.16		1.6	0.20	2−6MR, Cu-IE
Cu−CHA(0.23)	8.8	0.19		1.9	0.23	2−6MR, Cu-IE
Cu−CHA(0.42)	8.8	0.34		3.3	0.42	2−6MR, Cu-IE
NH_4−Cu−CHA(0.16)	8.8	0.13		1.3	0.16	2−6MR, NH_4,[d] Cu-IE
Cu−CHA(0.11)	23	0.22		0.92	0.11	1−6MR[e]
Cu−CHA(0.04)	21	0.07		0.33	0.04	1−6MR
Na−Cu−CHA(0.12)	26	0.27	0.51	1.0	0.12	2−6MR-Cu[f]
Cu−CHA(0.13)	11	0.13		1.1	0.13	1−6MR
Cu−CHA(0.72)	12	0.76		5.7	0.72	1−6MR, 2 × Cu-IE
1Al−Cu−CHA	76	0.23		0.31	0.04	F[−g]
0Al−Cu−CHA	∞			1.0		IWI[h]

[a]Catalyst nomenclature is defined by extraframework cations present and composition where Cu−CHA(x) denotes an SSZ-13 catalyst with x Cu atoms per CHA cage. [b]2−6MR denotes a SSZ-13 synthesis with Na in the synthesis gel, following which the zeolite was ion-exchanged twice with NH_4NO_3 to remove Na. [c]Cu-IE denotes Cu was introduced via aqueous copper ion exchange. [d]NH_4 denotes that following ion-exchange with NH_4NO_3, the zeolite was not calcined to remove NH_3. [e]1−6MR denotes a SSZ-13 synthesis without Na in the synthesis gel and the direct incorporation of Cu using TEPA. [f]2−6MR-Cu denotes a SSZ-13 synthesis with Na present in the synthesis gel and the direct incorporation of Cu using TEPA [g]F^- denotes a SSZ-13 synthesis in fluoride media. [h]IWI denotes preparation via incipient wetness impregnation of a defect-free SSZ-13.

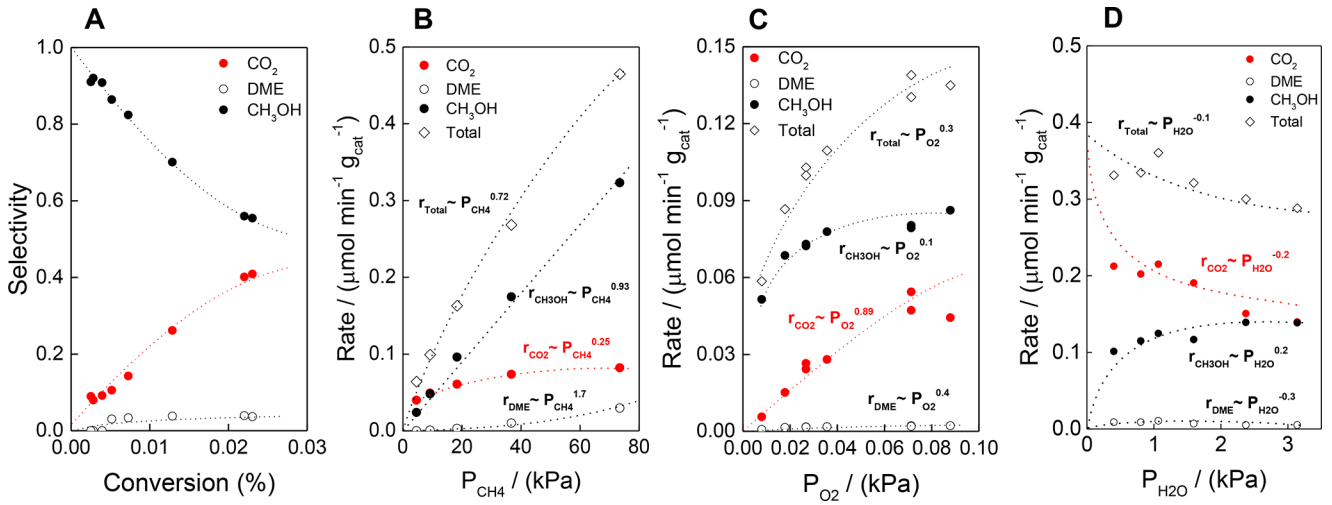

Figure 1. (A) Product selectivity as a function of conversion. Product formation rates as a function of (B) P_{CH4}, (C) P_{O2}, and (D) P_{H2O} variations over Cu−CHA(0.11). $r_{Total} = r_{CH3OH} + 2r_{DME} + r_{CO2}$, T = 543 K, 0.25 g_{cat}, 25−200 sccm total flow, P_{CH4} = 18 kPa, P_{O2} = 0.09 kPa, P_{H2O} = 3.14 kPa, bal He except as noted.

Herein, advanced synthesis techniques coupled with rigorous kinetic analysis and in situ spectroscopic characterization served to identify the active site responsible for the direct, steady-state catalytic conversion of CH_4 to methanol in copper-exchanged zeolites. Kinetic experiments performed on zeolites with the chabazite (CHA) topology, composed of 8 × 8 × 12 Å cages interconnected by windows with a maximum pore diameter of 3.8 Å,[32] uncovered a $[Cu−O−Cu]^{2+}$ dimeric motif as the active site for selective C−H activation. Zeolitic protons and H_2O are critical to the desorption of CH_3OH while being kinetically inconsequential. Cu dimers are hypothesized to form under reaction conditions by hydrated ionic diffusion along a protonic highway, highlighting the importance of zeolite H^+ content. Excess Cu (Cu/cage >0.3) resulted in Cu nanoparticle formation and consequently direct, complete oxidation of CH_4 to CO_2. The fundamental examination of CH_4 activation kinetics, site requirements, and conversion pathways provides a roadmap for the optimization of low-temperature CH_4-to-methanol technologies.

RESULTS AND DISCUSSION

1. Reaction Pathway for Catalytic Partial CH_4 Oxidation over a Cu Active Site. Investigation of active-site requirements for the direct conversion of CH_4 to methanol necessitates control of Cu ion speciation and, therefore, aluminum distribution, within the zeolite. We employed select synthetic methods to create a suite of catalysts with varied Cu content and Al speciation to study the effects of Cu distribution on C−H activation.[34,35] Synthesis, character-

DOI: 10.1021/jacs.9b04906
J. Am. Chem. Soc. 2019, 141, 11641−11650

ization, and catalyst compositional details are given in section 1 of the Supporting Information and Table 1. Catalysts designated as Cu−CHA(x) are copper-exchanged SSZ-13 zeolites with x Cu atoms per 8 × 8 × 12 Å cage.

Reaction rates were measured under kinetic control (Figures S1−S3 and Table S1). Reaction conditions were chosen to produce CH_3OH, DME, and CO_2 in yields large enough to aid in reaction pathway analysis, even though over 95% selectivity to CH_3OH can be achieved via reaction condition and catalyst choice (Figure S4). A first-order delplot constructed from a contact−time kinetic study of a representative catalyst (Cu−CHA(0.11), Figure 1A) indicates a sequential reaction pathway in which CH_4 can be first partially oxidized to CH_3OH before secondary downstream oxidation to CO_2.

Accordingly, the total rate of C−H activation was analyzed as the carbon-weighted sum of all products formed (r_{total} = r_{CH3OH} + 2r_{DME} + r_{CO2}). Kinetic analysis revealed a near first-order dependence of the C−H activation rate on P_{CH4} (Figure 1B), implying weak binding of CH_4 to the active site. The near second-order dependence of DME formation rates on P_{CH4} is consistent with a bimolecular dehydration of methanol over bare Brønsted acid sites. C−H activation rates exhibited a near zero-order dependence on P_{O2}, while CO_2 formation rates exhibited a linear dependence on O_2 partial pressure at P_{O2} < 0.1 kPa (Figure 1C), suggesting that the overoxidation process involves direct reaction of a C_1 intermediate with either unbound O_2 or with a low-coverage of O_2-derived species. The weak dependence of C−H activation on P_{O2} indicates that the reoxidation of Cu-active sites prior to C−H activation in the redox cycle is not rate-limiting.

Total C−H activation rates were nearly uninhibited by H_2O partial pressure (Figure 1D), and the partial oxidation selectivity decreased with decreasing water partial pressure to the limit of 0% in the absence of a H_2O cofeed (Figure S5). These results implicate a reaction pathway where a rate-determining C−H scission event catalyzed by an oxidized copper−oxygen species is followed by either (i) H_2O-facilitated methanol desorption or (ii) secondary oxidation of a C_1 intermediate to CO_2. Previous reports have hypothesized that H_2O substantially decreases the desorption energy of surface-bound methoxy species to form methanol after initial C−H scission events.[33,36−39] Lower partial pressures of H_2O decrease the probability of methanol desorption events, resulting in more frequent interactions of activated C_1 intermediates with gas phase O_2 and increased total oxidation (Figure 1D). The apparent activation energy of C−H scission was 97 kJ mol^{-1} (Figure S6). This barrier, indicative of the energetic difference between gas phase reactants and the transition state due to measurement in the P_{CH4} first-order regime, is in close accordance with density functional theory-calculated C−H activation barriers reported by Zhao et al.[37] over Cu active sites in mordenite zeolites and other similar work.[37,40] The hypothesized rate-determining C−H scission is in agreement with the previously reported primary kinetic isotope effect during steady state methane-to-methanol reactions using CD_4 over Cu-ZSM-5 catalysts.[28]

Similar kinetic experiments were performed using the 14 Cu−CHA samples listed in Table 1, whose Al speciation and Cu/Al compositions were controlled synthetically to probe the impacts of metal loading and Cu site speciation upon kinetics and product selectivity. All catalysts generally exhibited an increasing degree of undesirable downstream oxidation events with increasing conversion (Figure 2A) as expected from the

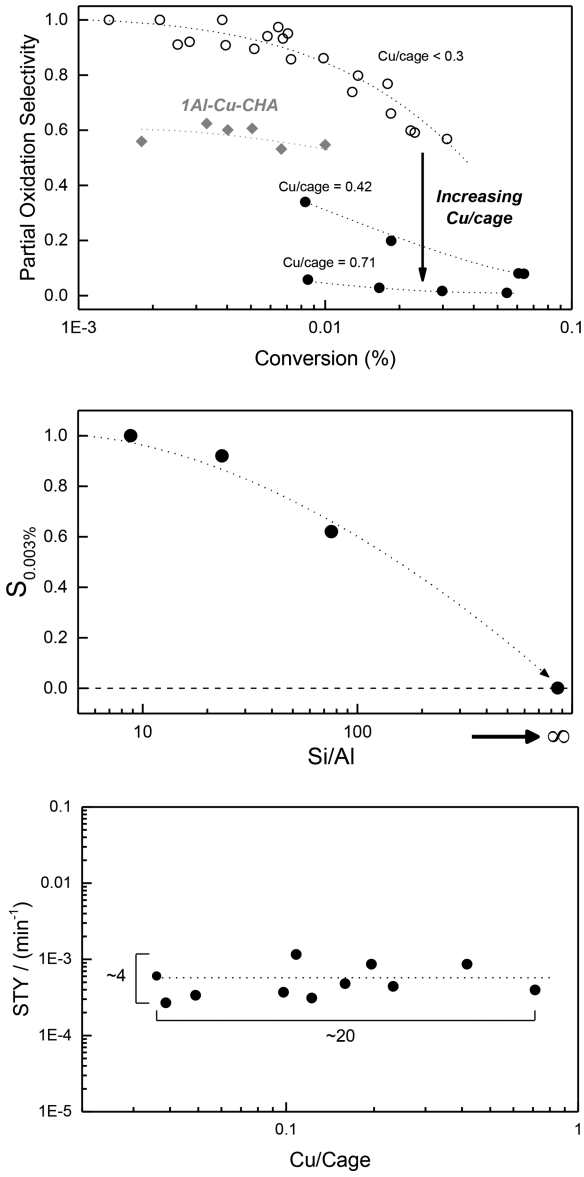

Figure 2. (A) Selectivity as a function of CH_4 conversion for separate catalyst samples. All catalyst properties are listed in Table 1. (B) Partial oxidation selectivity at 0.003% conversion versus decreasing Al content for four catalyst samples. (C) Cu-normalized total product formation rates (Site time yield, STY) as a function of Cu/cage. Reaction conditions: 0.25 g_{cat}, 543 K, 25−200 sccm total flow, P_{CH4} = 18 kPa, P_{O2} = 0.09 kPa, P_{H2O} = 3.14 kPa, bal He.

hypothesized sequential conversion pathway. Catalysts with Cu/cage >0.3 exhibited lower partial oxidation selectivity than expected based on sequential conversion, suggesting that higher Cu loadings direct the formation of active sites that are unselective toward methane partial oxidation. The purely siliceous 0Al−Cu−CHA sample, which lacked $[AlO_4]^-$ T-sites necessary for directing Cu ion exchange, only contained CuO_x nanoparticles within the CHA pores. This Al-free sample displayed broad UV−vis features in the 20000 and 40000 cm^{-1} regions that are associated with copper oxide nanoparticles (Figure S7).[41,42] This catalyst also exhibited the highest apparent activation energy (140 kJ mol^{-1}) of all measured catalysts and near 0% selectivity to CH_3OH. Al-containing catalysts with increasing Cu content above Cu/cage >0.3 also exhibited increasing apparent activation energies, similar UV−

DOI: 10.1021/jacs.9b04906
J. Am. Chem. Soc. 2019, 141, 11641−11650

vis features to those observed in 0Al−Cu−CHA (Figure S7, Table S2) and low partial oxidation selectivity, implicating the onset of CuO_x nanoparticle formation when exceeding a copper loading of Cu/cage = 0.3.

In addition, a sample with a low Al content (1Al−Cu−CHA, Si/Al = 76) was synthesized to isolate, on average, 1 Al T-site for every ∼3 cages (one CHA cage consists of 36 T-sites that are each shared between three cages). This sample featured only ∼50% selectivity to methanol with Cu/cage <0.2, a sub-first-order dependence of the total rate on P_{CH4}, and a first-order dependence of the total rate on P_{O2} (Figures 2A, S9, and S10), differing significantly from all other Cu−CHA zeolites investigated. Spectroscopic studies of 1Al−Cu−CHA under working conditions indicated the presence of isolated Cu sites (vide infra). To further illustrate the effect of the Si/Al ratio, Figure 2B compares partial oxidation selectivity of four catalysts of differing Al content and similar Cu loadings below Cu/cage = 0.2 at isoconversion (0.003%). Decreasing Al content resulted in decreased selectivity for partial oxidation (Figures 2B and S12), underscoring the importance of zeolitic H^+ species in the turnover cycle (vide infra). Moreover, a fully siliceous zeolite without ion-exchanged Cu species present displayed 0% selectivity toward methanol (0Al−Cu−CHA, Figure S8), suggesting that partial oxidation of methane requires ion-exchanged Cu species within the zeolite.

Figure 2C shows the overall site time yield across all catalysts (STY; the total rate of C−H activation normalized by Cu content) varied by a factor of 4 over a span of Cu loading that varied by a factor of 20. This minimal variation in STY across a large range of Cu loadings in conjunction with similar kinetic pressure dependences and energetic barriers (Table S2) implies the mechanisms and energetics of C−H activation are similar across numerous Cu-centric active sites, excluding 1Al−Cu−CHA. Slight variations in STY and kinetic dependences may be indicative of a subset of Cu species in some catalyst samples that are either inactive for C−H activation or distinct from the selective partial oxidation sites present in Cu/cage < 0.3 samples. These results highlight the necessity of moderate Cu loadings and high Al content to direct the synthesis of well-dispersed partial oxidation active sites.

2. Effects of Pretreatment, Brønsted Acidity, and NH_3 on CH_4 Oxidation. Inspired by reports on the mobilization of ammonia-solvated $[H_3N−Cu−NH_3]^+$ species to form multinuclear copper active sites in SSZ-13 at 473 K under NO_x reduction conditions,[43−45,46,47] we applied similar reductive and oxidative pretreatments to gain insight into the nature of the formation and turnover of active sites for CH_4 oxidation on Cu−CHA(0.23). As shown in Figure 3A, oxidative and reductive pretreatments had minimal effects on steady-state rates with one notable exception: NH_3 severely decreased the rate of C−H activation whether introduced during pretreatment or as a cofeed, and these rates could not be entirely recovered upon removal of the NH_3 cofeed (Figure 3A). These inhibitive effects can be attributed to the favorable adsorption of NH_3 to both Brønsted acid sites and extraframework Cu ions within the zeolite pores.[34,48−50]

To probe the effects of NH_3 on C−H activation, we performed an operando NH_3 titration (Figure 3B) over Cu−CHA(0.23) under the following conditions: (i) baseline steady-state flows (SS), (ii) NH_3 cofeed with steady-state flows (SS + NH_3), (iii) steady-state flows after removal of the NH_3 titrant (SS post NH_3), and (iv) baseline steady-state flows after heating the catalyst to 673 K and holding for >10 h under

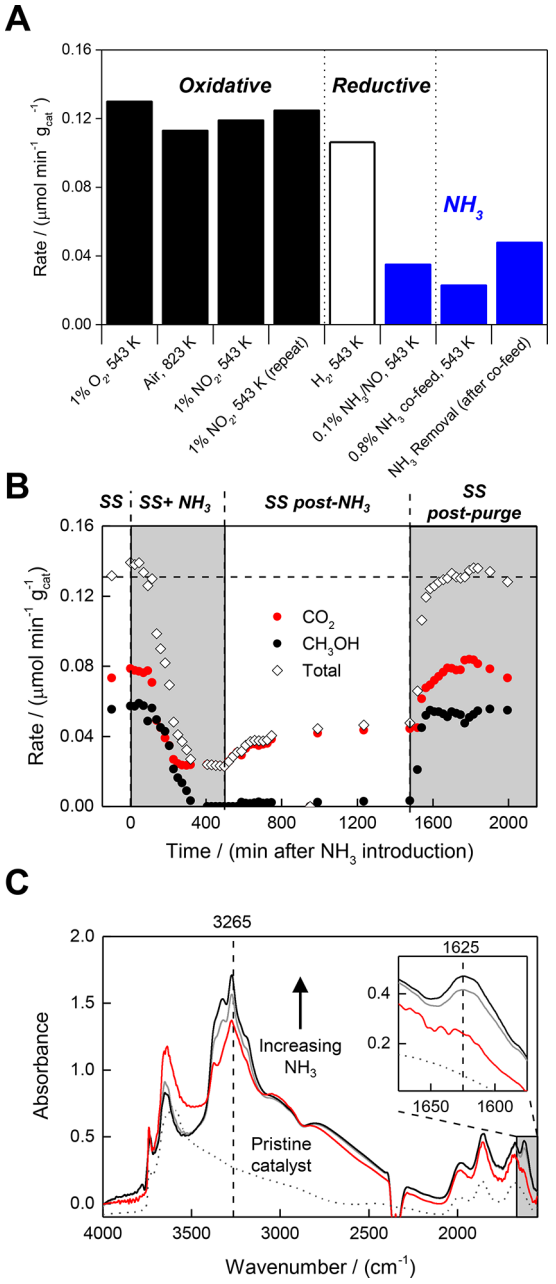

Figure 3. Effect of NH_3 on catalytic methanol formation and Cu speciation for Cu−CHA(0.23). (A) Product formation rates versus pretreatment conditions and NH_3 cofeed as listed. (B) Effect on methanol formation. (C) Ex situ FTIR of two catalyst samples: (i) "Fresh" Cu−CHA(0.23), never exposed to reaction conditions, only exposed to helium at 543 K, and (ii) Cu−CHA(0.23) exposed to methanol synthesis flows, NH_3 cofeed, and removal of NH_3 cofeed before being removed from the reactor, pelletized, placed in the IR cell, and treated with subsequent in situ dosing with NH_3. CH_4 activation conditions were 0.25 g_{cat}, 543 K, 25 sccm, P_{CH4} = 18 kPa, P_{O2} = 0.09 kPa, P_{H2O} = 3.14 kPa, bal He. P_{NH3} = 0.08 kPa when cofeeding NH_3. Spectra were collected in transmission of a 10 mg, 7 mm self-supporting catalyst wafer at 543 K under flowing dry He. NH_3 was introduced by pulses of 0.4 μmol NH_3 in He.

pure helium flow (SS post-purge). Upon introduction of an NH_3 cofeed, methanol synthesis was almost entirely suppressed and CO_2 formation rates were substantially decreased (Figure 3B, left). Removal of the NH_3 cofeed resulted in a moderate increase in CO_2 formation rates, but methanol

DOI: 10.1021/jacs.9b04906
J. Am. Chem. Soc. 2019, 141, 11641−11650

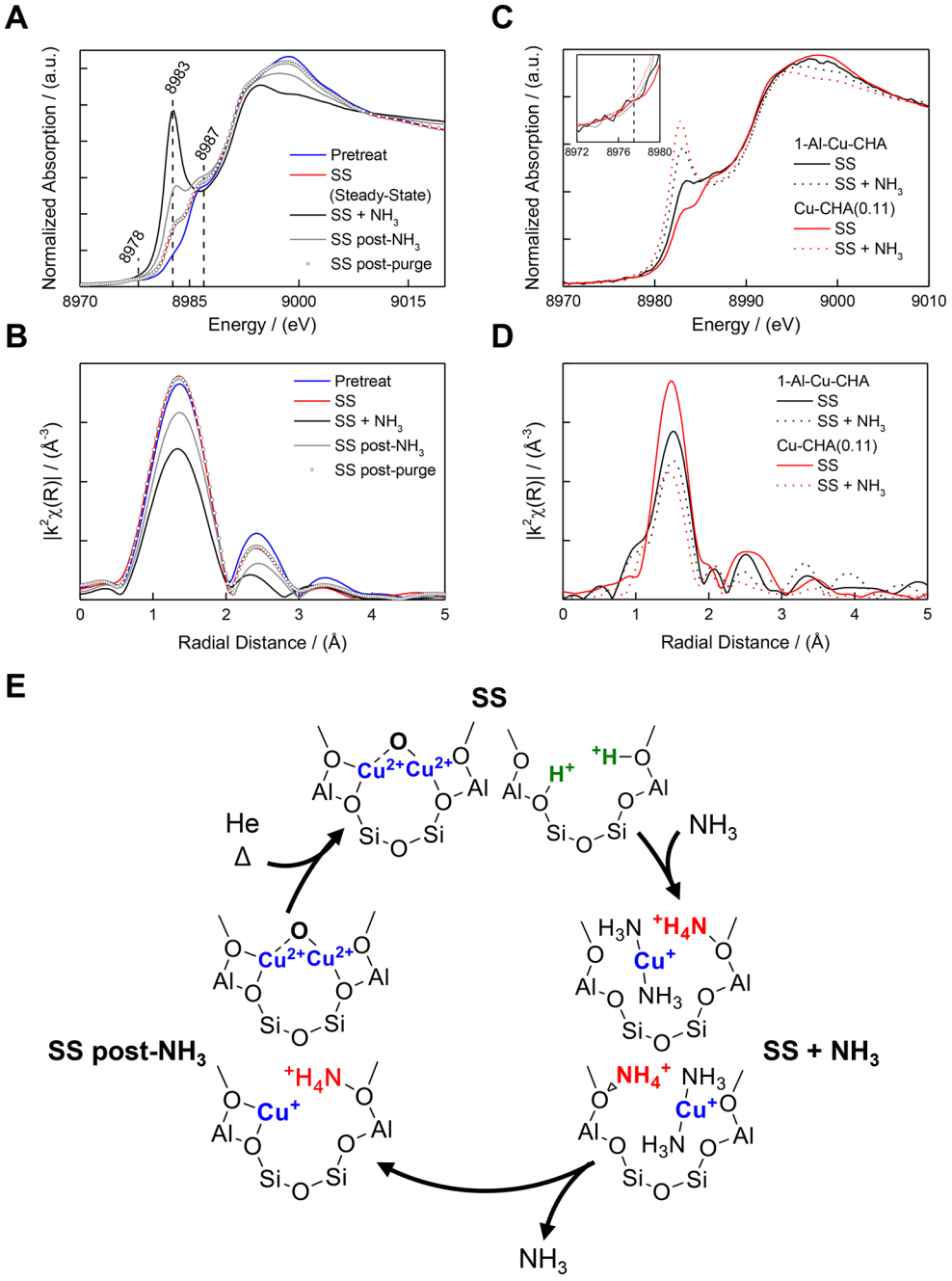

Figure 4. (A) XANES and (B) EXAFS of Cu−CHA(0.11) and (C) XANES and (D) EXAFS of 1Al−Cu−CHA and Cu−CHA(0.11) under methanol synthesis and NH_3 flows. All spectra were collected at 543 K. The catalyst was pretreated in 1 kPa O_2, bal He from 298 to 543 K at 5 K min^{-1} (pretreat). At 543 K, the catalyst was exposed to methanol synthesis flows of P_{CH4} = 18 kPa, P_{O2} = 0.09 kPa, P_{H2O} = 3.14 kPa, bal He (SS), an additional NH_3 cofeed of P_{NH3} = 0.16 kPa (SS + NH_3), and then the removal of NH_3 (SS post-NH_3). Following NH_3 removal, the catalyst was brought to 673 at 6 K min^{-1} and held in dry He before cooling to 543 K and exposure to methanol synthesis flows (SS post-purge). (E) Hypothesized schematic representations of the average states of charge balancing Cu, NH_4^+, and H^+ species as a function of reaction flows and treatments. Single O atoms may correspond to framework zeolite O atoms or coordinating H_2O molecules.

production rates did not recover to the original values (Figure 3B, middle). Di Iorio et al. reported that upon adsorption of NH_3 to both Brønsted acid sites and Cu, treatment with a wet He flow at 433 K selectively desorbed NH_3 from Cu without perturbing NH_3 coordinated to zeolitic protons.[48] Upon removal of the NH_3 cofeed in our system, the $CH_4/O_2/H_2O$ stream contacted the NH_3-titrated catalyst for ∼1000 min at 543 K, conditions that selectively removed NH_3 only from Cu sites. This result is a strong indication that the persistent, significant inhibition of C−H activation rates after NH_3 removal was due to the blocking of Brønsted acid sites and not attributable to the blockage of Cu ions. An extended 12 h treatment under flowing helium at 673 K, known to induce NH_3 desorption even from zeolitic protons,[48] resulted in full recovery of CH_4 conversion rates and selectivity values (Figure 3B, right), further evincing the deleterious effects of proton blocking.

The necessity of protons for methanol production was inferred from the negligible selectivity to methanol shown in the center of Figure 3B (SS post-NH_3), conditions under

DOI: 10.1021/jacs.9b04906
J. Am. Chem. Soc. 2019, 141, 11641−11650

which NH_3 inhibits protons but not Cu as discussed above. Moreover, increasing the extent of NH_3 titration (leading to decreasing conversion) did not result in increasing selectivity to methanol as expected from Figure 2A. Thus, we hypothesize that the absence of H^+ on Al sites impedes either (i) the formation of selective active sites or (ii) the desorption of methanol from selective active sites (if these sites remain). A combination of these two factors is also possible. Rapid regeneration of methanol synthesis rates upon NH_3 purging (Figure 3B, SS post-purge) and the partial similarities of spectroscopic features of Cu species under SS and SS post-NH_3 conditions (vide infra) imply some fraction of selective partial methane oxidation active sites were present under SS post-NH_3 conditions, implicating the importance of H^+ for CH_3OH desorption.

Cu−CHA(0.23) was also characterized ex situ by FTIR spectroscopy following exposure and subsequent removal of an NH_3 cofeed under reaction conditions (Figure 3C, red trace, SS post-NH_3). A strong signal from NH_3 adsorbed to Brønsted acid sites (3265 cm^{-1}) was observed while a signal from NH_3 adsorbed to Cu (1625 cm^{-1}) was entirely absent (Figure 3C, peak assignment in Figure S11). Neither of these features were observed on a fresh Cu−CHA(0.23) that was not exposed to reaction conditions or NH_3 dosing (dotted trace, fresh). Next, the SS post-NH_3 Cu−CHA(0.23) sample was subjected to a series of 0.4 μmol NH_3 in He pulses, resulting in the appearance of both Cu−NH_3 signatures and more prominent NH_4^+ features (Figure 3C), confirming the selective desorption of NH_3 from Cu and minimal desorption from Brønsted acid sites after NH_3 cofeed removal under reaction conditions. The importance of zeolitic protons on C−H activation was also highlighted when testing catalysts where framework acid sites were ion-exchanged with NH_4^+ or Na^+ (Figures S12 and S13). Both of these ions inhibit methanol formation and appear to decrease the total rate of C−H activation. Although all of the effects of NH_4^+ and Na^+ ions on partial methane oxidation rates and selectivity cannot be conclusively proven to be identical, both ions cause similar effects to those observed from NH_3 cofeed-induced H^+ inhibition.

Taken together, these data show Brønsted acid site blocking has a twofold effect: (i) near complete inhibition of methanol formation pathways and (ii) significant inhibition of either C−H or O_2 activation processes. Figure 2C shows the rate of C−H activation is relatively invariant across samples of varying Al content (8.8 < Si/Al < 76). Therefore, we posit that protons are not kinetically relevant to the rate-determining C−H activation step. However, given the suppression of total CH_4 conversion due to H^+-inhibition, Brønsted acid sites are necessary for the completion of a C−H activation catalytic cycle, possibly by enabling active-site formation or reoxidation.

The interrelation between Cu speciation, Brønsted acid sites, and NH_3 was investigated by in situ X-ray absorption spectroscopy (XAS) during an identical NH_3 titration experiment to that shown in Figure 3B. The effects of Al-density within the zeolite framework were also probed using two representative catalysts of similar Cu content: (i) high Al content (Cu−CHA(0.11)) and (ii) low Al content (1Al−Cu−CHA). Parts A and B of Figure 4 show the XAS spectra of the high-Al content Cu−CHA(0.11) during an entire NH_3 titration experiment; fitting of the extended X-ray absorption fine structure (EXAFS) of Cu−CHA(0.11) upon exposure to steady-state methanol synthesis conditions agrees with a $[Cu-O-Cu]^{2+}$ motif (fits of all spectra are summarized in Figure S14 and Table S3). The XANES spectra indicated the presence of both Cu(I) (8983 eV[51]) and Cu(II) (8978 and 8987 eV[51]), consistent with a Cu(II)/Cu(I) redox cycle during C−H activation. The first shell scattering peak fit to a Cu−O coordination number (CN) of 3.1 ± 1.1 (R_{Cu-O} = 1.90 ± 0.02 Å), and the second shell scattering peak fit to a Cu−Cu CN of 1.1 ± 0.6 (R_{Cu-Cu} = 2.94 ± 0.05 Å). These values are consistent with a moiety where each Cu atom coordinates to two framework O atoms or coordinating H_2O molecules, one extraframework O atom, and an additional Cu atom, represented in Figure 4E. The observed interatomic distances for both Cu−O and Cu−Cu are also consistent with distances calculated for Cu dimers in SSZ-13,[52] yet we also recognize that the uncertainty of the Cu−O CN does not preclude the presence of either a Cu dimer coordinating to two extraframework O atoms or a subset of nondimeric Cu species. Fitting of the second shell EXAFS peak with a T-site resulted in a negative CN (Table S4). However, given the overlap of Cu−T-site and Cu−Cu scattering, small contributions by a T-site cannot be ruled out. In situ UV−vis experiments of Cu−CHA(0.11) display a feature centered around 37500 cm^{-1} that is present under methanol synthesis flows and not present upon titration with NH_3 (Figure S15). Li et al. calculated features in this region that can be attributed to Cu dimers in SSZ-13.[53] Definitive assignment of this band is inconclusive, however, as features in this region may simply be related to reduction and oxidation of Cu ions.[24] These results fall in line with an abundant, oxidized dimeric Cu-active site present at steady state prior to a rate-determining C−H activation event.

NH_3 cofeed (SS + NH_3) resulted in the generation of a strong Cu(I) pre-edge feature, the disappearance of both Cu(II) pre-edge features (Figure 4C inset), the disappearance of the Cu−Cu scattering signal, and a decrease in the first shell coordination number (CN) from 3.1 ± 1.1 to 1.8 ± 0.3. These changes are consistent with the destruction of Cu dimers and the formation of mobile $[H_3N-Cu-NH_3]^+$ species similar to those previously reported by Paolucci et al. and represented in Figure 4E.[46] Removal of the NH_3 cofeed (SS post-NH_3) resulted in a partial recovery in both the Cu−O and Cu−Cu scattering signals and a partial decrease in the intensity of the Cu(I) pre-edge feature.

As discussed previously, NH_3 remains bound to Brønsted acid sites under methanol synthesis conditions after removal of the NH_3 titrant, demonstrating that zeolitic protons are crucial for both Cu reoxidation and reformation of Cu dimers for a significant fraction of Cu ions. In the final step of the titration experiment, initial steady-state Cu speciation was restored after purging NH_3 from zeolitic protons under helium flow at 673 K and subsequently reintroducing methanol synthesis flows.

Parts C and D of Figure 4 compare the effects of NH_3 titration on low- and high-Al content samples via in situ XAS under the same methanol synthesis and NH_3 titration conditions. 1Al−Cu−CHA exhibits a stronger Cu(I) pre-edge feature under steady-state methanol synthesis conditions versus Cu−CHA(0.11). A fit of the EXAFS of 1Al−Cu−CHA (Figure 4D, Figure S16, and Table S5) under these same conditions provided a Cu−O CN of 1.8 ± 0.5 (R_{Cu-O} = 1.94 ± 0.02 Å) and a smaller Cu−Cu CN of 0.6 ± 0.3 (R_{Cu-Cu} = 2.9 ± 0.1 Å) compared to Cu−CHA(0.11). Due to the nature of XAS as a bulk averaging technique, a Cu−Cu coordination number less than 1 is indicative of a mixture of isolated Cu−O species and multinuclear Cu-oxo species. An NH_3 cofeed to 1Al−Cu−CHA yielded similar results as with Cu−

DOI: 10.1021/jacs.9b04906
J. Am. Chem. Soc. 2019, 141, 11641−11650

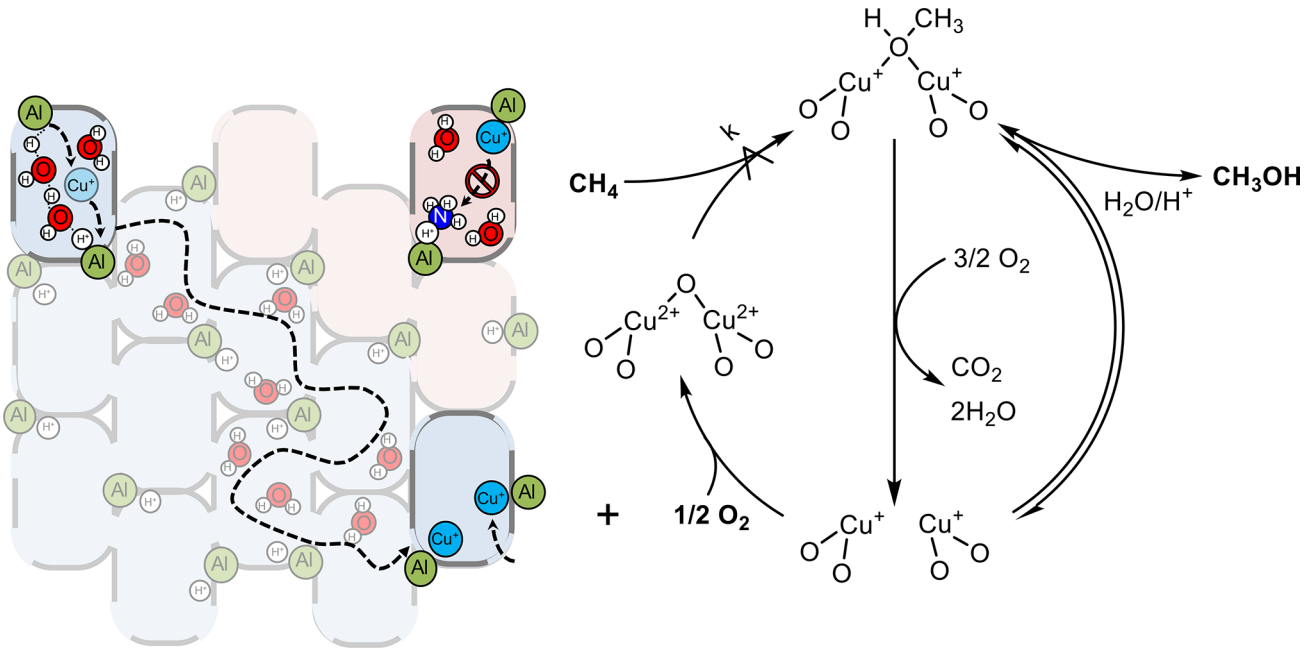

Figure 5. Depiction of hypothesized H^+/H_2O-aided diffusion of Cu^+ and NH_3 inhibition within SSZ-13 to form Cu dimers relevant to the proposed catalytic methane oxidation cycle. Single O atoms may correspond to framework zeolite O atoms or coordinating H_2O molecules.

CHA(0.11): only Cu(I) was observed, Cu−O scattering intensity was reduced, and Cu−Cu scattering was eliminated. These results imply that an increasingly sparse Al population decreases the likelihood of multinuclear Cu species even at a moderate Cu/Al loading and that isolated Cu species cannot be facilely aerobically oxidized.

Because of its bulk sampling nature, EXAFS alone cannot identify the active site for selective partial methane oxidation. However, EXAFS in combination with the reactivity measurements and NH_3 titration experiments indicate a Cu dimer active site is the likely catalytically active site for continuous selective partial oxidation of methane to methanol. Therefore, these combined reactivity and in situ spectroscopic data support the hypothesis that a $[Cu-O-Cu]^{2+}$ motif acts as the active site for catalytic partial CH_4 oxidation in SSZ-13, the dimer is formed at low Cu loadings (Cu/cage < 0.3), and free zeolitic protons are critical for Cu dimer formation as evinced from selective synthesis, spectroscopic, and NH_3 titration results.

3. Proposed Mechanism for $[Cu-O-Cu]^{2+}$ Motif Formation. The formation of a $[Cu-O-Cu]^{2+}$ moiety as the selective oxidation active site is puzzling given partial oxidation was observed at Cu densities as low as 0.04 Cu/cage where the probability of having two Cu ions within the same cage is prohibitively small. Further, while the partial methane oxidation selectivities of Cu−CHA(0.05) and Cu−CHA(0.04) were near unity (Figure 2A), the selectivity for methanol of 1Al−Cu−CHA was much lower despite similar Cu/cage values among the three catalysts (0.05, 0.04, and 0.04 respectively), demonstrating that the active sites for selective partial oxidation form when the zeolite Al-content is sufficiently high even when the Cu loading is low. However, we stress that high Cu loadings lead to nonselective active species regardless of Al content as depicted above. In situ NH_3 titrations and concurrent spectroscopic data clearly show that Brønsted acid sites are involved in the formation of the $[Cu-O-Cu]^{2+}$ motif. We posit that these results can be rationalized by considering the proton-aided diffusion of hydrated Cu ions within the CHA framework schematically represented in Figure 5; this hypothesized process is fundamentally analogous to the putative mechanism that allows hydrated Cu ions to diffuse into and out of CHA cages during aqueous ion exchanges.

Each framework T-site in CHA is shared among three neighboring cages, and extraframework cations (e.g., H^+, Cu^+, Cu^{2+}) coordinated to Al T-sites can readily access each of these cages via the 8-MR windows with a minimal energetic penalty.[46] Psofogiannakis et al. used force field/molecular dynamics simulations to demonstrate that tetra-hydrated Cu ions are fully desorbed from the SSZ-13 framework and mobile on the picosecond time scale at temperatures relevant to this work (500−700 K). Further, Paolucci et al. calculated an energetic barrier of ∼35 kJ mol^{-1} for the rotation of $[H_3N-Cu-NH_3]^+$ species through an 8MR window to an adjacent cage.[46,54] Assuming a Cu ion can be mobilized and transferred to a proximate $[AlO_4]^-$ T-site, charge balance can be maintained by water-assisted proton hopping (Figure 5, top left). A zeolite with a high enough Al content, combined with the H^+/H_2O/Cu ion-exchange process and Cu ion rotation between CHA cages would effectively allow Cu ions to access the entirety of the zeolite framework and facilitate Cu ion pairing even in low Cu-content zeolites. This Cu ion mobility thus enables the formation of thermodynamically favorable Cu dimer species in the presence of water.[34,54]

The low energetic barrier for this ion exchange across a single CHA cage and the facile shifting of Cu ions and protons between neighboring cages provide a means for Cu ions to access the entire microporous zeolite when a sufficiently high Al content allows for Cu ion exchange between nearby $[AlO_4]^-$ T-sites.[55] The introduction of NH_3 into the zeolite disperses Cu species as mobile $[H_3N-Cu-NH_3]^+$ and simultaneously blocks protons by NH_4^+ formation. Upon removal of NH_3 cofeed, Cu ions are deposited on $[AlO_4]^-$ T-sites, but now NH_4^+ (and not H^+) ions are coordinated to $[AlO_4]^-$ sites that lack Cu ions. These NH_4^+ ions are too

DOI: 10.1021/jacs.9b04906
J. Am. Chem. Soc. 2019, 141, 11641−11650

energetically stable to desorb from $[AlO_4]^-$ T-sites to facilitate Cu ion mobility (Figures 4 and 5).

Aerobic oxidation of Cu to selectively produce methanol is hypothesized to necessitate dimeric species in contrast to the facile and complete oxidation of both monomeric and dimeric Cu(I) achieved by an NO_2 pretreatment (Figure S17).[34] Thus, catalytic CH_4 partial oxidation is greatly hindered without Cu dimer formation via an available ion diffusion pathway. The increased presence of Cu(I) following removal of the NH_3 cofeed observed in Figure 4A (SS post-NH_3) compared to the original methanol synthesis flows (SS) is explained by the inability of O_2 to oxidize all isolated Cu(I) when the latter is trapped by NH_4^+ (Figure 5, top right cage of left scheme). The fraction of isolated Cu species oxidized by O_2 are thought to account for the non-zero rate of CO_2 formation in the presence of NH_3 and following NH_3 removal. Only upon complete NH_3 desorption and reintroduction of methanol synthesis flows is this significant fraction of Cu(I) reoxidized and C−H activation rates restored. This coincides with the opening of ionic diffusive channels that result in reformation of dimeric Cu active sites.

This theory is corroborated by the results in Figure 4C,D of the isolated Al 1Al−Cu−CHA sample; this sample exhibits predominantly isolated Cu−O species that cannot diffuse due to a sparse population of $[AlO_4]^-$ T-sites. In line with this assumption, EXAFS analysis of the 1Al−Cu−CHA sample revealed limited Cu−Cu scattering (Figure 4D). Cu dimer formation in a zeolite with low Al content can be accounted for by pockets of proximate Al sites, resulting from either (i) a random Al distribution (the average Al−Al distance at this Si/Al is 1.7 nm, close enough to permit Cu dimer formation via the 0.9 nm maximum diffusion radius of a Cu ion[46]) or (ii) Al zoning formed during zeolite synthesis as previously observed in other frameworks.[56,57] Furthermore, the increased intensity of the Cu(I) pre-edge feature of 1Al−Cu−CHA (Figure 4C) is consistent with a greater population of isolated Cu−O species. However, partial methane oxidation activity over isolated Cu species cannot be ruled out. The Cu speciation and distinct kinetics of 1Al−Cu−CHA are still under investigation. While this mechanism is not unequivocally proven, the comprehensive and complex results reported in this work can be simply rationalized via an ionic diffusion pathway that facilitates the formation of $[Cu-O-Cu]^{2+}$ motifs that are active for selective partial oxidation of CH_4.

CONCLUSIONS

The reaction pathway and active site for the direct conversion of CH_4 to methanol over Cu-SSZ-13 was elucidated with kinetic experiments in combination with spectroscopic techniques. Low Cu loadings (Cu/cage < 0.3) with sufficiently high Al content (Si/Al > 30) are critical to direct the speciation of a $[Cu-O-Cu]^{2+}$ motif that catalyzes selective CH_4 partial oxidation while avoiding formation of other Cu structures and Cu_xO_y nanoclusters that promote complete CH_4 oxidation to CO_2. CH_4 activation proceeds via rate-determining C−H scission to form a surface-bound C_1 intermediate that can either be desorbed as methanol in the presence of H_2O/H^+ or completely oxidized to CO_2 by gas-phase O_2. Importantly, the $[Cu-O-Cu]^{2+}$ motif is hypothesized to form via the diffusion of hydrated Cu ions along a proton-paved highway. High partial oxidation selectivity can be targeted by utilizing (i) reaction conditions of high CH_4 and water partial pressure and (ii) catalysts containing a high density of Brønsted acid sites and moderate Cu loadings (Cu/cage < 0.3) to maximize the speciation of dimeric Cu moieties. This work highlights the importance of developing mechanistic understanding to direct both synthesis-driven active site speciation and reaction condition selection for process optimization.

METHODS

See the Supporting Information for a detailed Methods section.

ASSOCIATED CONTENT

Supporting Information

The Supporting Information is available free of charge on the ACS Publications website at DOI: 10.1021/jacs.9b04906.

All experimental methods, catalyst characterization, and supporting figures referenced in the main text (PDF)

AUTHOR INFORMATION

Corresponding Author

*E-mail: yroman@mit.edu.

ORCID

Kimberly T. Dinh: 0000-0003-0657-1771
Mark M. Sullivan: 0000-0002-1765-4129
Randall J. Meyer: 0000-0002-0679-0029
Yuriy Román-Leshkov: 0000-0002-0025-4233

Author Contributions

‖K.T.D. and M.M.S. contributed equally.

Notes

The authors declare no competing financial interest.

ACKNOWLEDGMENTS

The authors gratefully acknowledge the financial support of ExxonMobil. K.D. acknowledges the partial support from the National Science Foundation Graduate Research Fellowship under Grant No. 1122374. Any opinions, findings, and conclusions or recommendations expressed in this material are those of the author(s) and do not necessarily reflect the views of the National Science Foundation. MRCAT operations are supported by the Department of Energy and the MRCAT member institutions. This research used resources of the Advanced Photon Source, a U.S. Department of Energy (DOE) Office of Science User Facility operated for the DOE Office of Science by Argonne National Laboratory under Contract No. DE-AC02-06CH11357. This work made use of the MRSEC Shared Experimental Facilities at MIT, supported by the National Science Foundation under Award No. DMR-14-19807. The authors thank Z. Wang for help in ICP data collection, J. Katsoudas, T. Wu, and S. Aryal for help with XAS data collection, M. Stone and T. Gani for comments on the manuscript, and A. Stubbs and X. He for helpful discussions.

REFERENCES

(1) Kondratenko, E. V.; Peppel, T.; Seeburg, D.; Kondratenko, V. A.; Kalevaru, N.; Martin, A.; Wohlrab, S. Methane conversion into different hydrocarbons or oxygenates: current status and future perspectives in catalyst development and reactor operation. *Catal. Sci. Technol.* **2017**, *7* (2), 366−381.

(2) Ahlquist, M.; Nielsen, R. J.; Periana, R. A.; Goddard, W. A., III Product Protection, the Key to Developing High Performance Methane Selective Oxidation Catalysts. *J. Am. Chem. Soc.* **2009**, *131* (47), 17110−17115.

DOI: 10.1021/jacs.9b04906
J. Am. Chem. Soc. 2019, 141, 11641−11650

(3) Shilov, A. E.; Shul'pin, G. B. Activation of C−H Bonds by Metal Complexes. *Chem. Rev.* **1997**, *97* (8), 2879−2932.
(4) Tan, S. H.; Barton, P. I. Optimal dynamic allocation of mobile plants to monetize associated or stranded natural gas, part I: Bakken shale play case study. *Energy* **2015**, *93* (2), 1581−1594.
(5) *International Energy Outlook 2016*; U.S. Energy Information Administration: Washington, DC, May 11, 2016; pp 37−60.
(6) Snyder, B. E. R.; Bols, M. L.; Schoonheydt, R. A.; Sels, B. F.; Solomon, E. I. Iron and Copper Active Sites in Zeolites and Their Correlation to Metalloenzymes. *Chem. Rev.* **2018**, *118* (5), 2718−2768.
(7) Ciano, L.; Davies, G. J.; Tolman, W. B.; Walton, P. H. Bracing copper for the catalytic oxidation of C−H bonds. *Nat. Catal.* **2018**, *1* (8), 571−577.
(8) Solomon, E. I.; Heppner, D. E.; Johnston, E. M.; Ginsbach, J. W.; Cirera, J.; Qayyum, M.; Kieber-Emmons, M. T.; Kjaergaard, C. H.; Hadt, R. G.; Tian, L. Copper active sites in biology. *Chem. Rev.* **2014**, *114* (7), 3659−3853.
(9) Lieberman, R. L.; Rosenzweig, A. C. Crystal structure of a membrane-bound metalloenzyme that catalyses the biological oxidation of methane. *Nature* **2005**, *434* (7030), 177−82.
(10) Balasubramanian, R.; Smith, S. M.; Rawat, S.; Yatsunyk, L. A.; Stemmler, T. L.; Rosenzweig, A. C. Oxidation of methane by a biological dicopper centre. *Nature* **2010**, *465* (7294), 115−119.
(11) Panov, G. I.; Sobolev, V. I.; Dubkov, K. A.; Parmon, V. N.; Ovanesyan, N. S.; Shilov, A. E.; Shteinman, A. A. Iron complexes in zeolites as a new model of methane monooxygenase. *React. Kinet. Catal. Lett.* **1997**, *61* (2), 251−258.
(12) Szécsényi, Á.; Li, G.; Gascon, J.; Pidko, E. A. Mechanistic Complexity of Methane Oxidation with H_2O_2 by Single-Site Fe/ZSM-5 Catalyst. *ACS Catal.* **2018**, *8* (9), 7961−7972.
(13) Groothaert, M. H.; Smeets, P. J.; Sels, B. F.; Jacobs, P. A.; Schoonheydt, R. A. Selective oxidation of methane by the bis(mu-oxo)dicopper core stabilized on ZSM-5 and mordenite zeolites. *J. Am. Chem. Soc.* **2005**, *127* (5), 1394−1395.
(14) Bozbag, S. E.; Alayon, E. M. C.; Pecháček, J.; Nachtegaal, M.; Ranocchiari, M.; van Bokhoven, J. A. Methane to methanol over copper mordenite: yield improvement through multiple cycles and different synthesis techniques. *Catal. Sci. Technol.* **2016**, *6* (13), 5011−5022.
(15) Dusselier, M.; Davis, M. E. Small-Pore Zeolites: Synthesis and Catalysis. *Chem. Rev.* **2018**, *118* (11), 5265−5329.
(16) Kosinov, N.; Liu, C.; Hensen, E. J. M.; Pidko, E. A. Engineering of Transition Metal Catalysts Confined in Zeolites. *Chem. Mater.* **2018**, *30* (10), 3177−3198.
(17) Kulkarni, A. R.; Zhao, Z.-J.; Siahrostami, S.; Norskov, J. K.; Studt, F. Cation-exchanged zeolites for the selective oxidation of methane to methanol. *Catal. Sci. Technol.* **2018**, *8* (1), 114−123.
(18) Woertink, J. S.; Smeets, P. J.; Groothaert, M. H.; Vance, M. A.; Sels, B. F.; Schoonheydt, R. A.; Solomon, E. I. A $[Cu_2O]^{2+}$ core in Cu-ZSM-5, the active site in the oxidation of methane to methanol. *Proc. Natl. Acad. Sci. U. S. A.* **2009**, *106* (45), 18908−18913.
(19) Grundner, S.; Luo, W.; Sanchez-Sanchez, M.; Lercher, J. A. Synthesis of single-site copper catalysts for methane partial oxidation. *Chem. Commun. (Cambridge, U. K.)* **2016**, *52* (12), 2553−2556.
(20) Grundner, S.; Markovits, M. A.; Li, G.; Tromp, M.; Pidko, E. A.; Hensen, E. J.; Jentys, A.; Sanchez-Sanchez, M.; Lercher, J. A. Single-site trinuclear copper oxygen clusters in mordenite for selective conversion of methane to methanol. *Nat. Commun.* **2015**, *6*, 7546−7555.
(21) Shan, J.; Li, M.; Allard, L. F.; Lee, S.; Flytzani-Stephanopoulos, M. Mild oxidation of methane to methanol or acetic acid on supported isolated rhodium catalysts. *Nature* **2017**, *551* (7682), 605−608.
(22) Huang, W.; Zhang, S.; Tang, Y.; Li, Y.; Nguyen, L.; Li, Y.; Shan, J.; Xiao, D.; Gagne, R.; Frenkel, A. I.; Tao, F. Low-Temperature Transformation of Methane to Methanol on Pd_1O_4 Single Sites Anchored on the Internal Surface of Microporous Silicate. *Angew. Chem.* **2016**, *128* (43), 13639−13643.
(23) Vanelderen, P.; Vancauwenbergh, J.; Sels, B. F.; Schoonheydt, R. A. Coordination chemistry and reactivity of copper in zeolites. *Coord. Chem. Rev.* **2013**, *257* (2), 483−494.
(24) Ipek, B.; Wulfers, M. J.; Kim, H.; Göltl, F.; Hermans, I.; Smith, J. P.; Booksh, K. S.; Brown, C. M.; Lobo, R. F. Formation of $[Cu_2O_2]^{2+}$ and $[Cu_2O]^{2+}$ toward C−H Bond Activation in Cu-SSZ-13 and Cu-SSZ-39. *ACS Catal.* **2017**, *7* (7), 4291−4303.
(25) Li, G.; Pidko, E. A. The Nature and Catalytic Function of Cation Sites in Zeolites: a Computational Perspective. *ChemCatChem* **2019**, *11* (1), 134−156.
(26) Mahyuddin, M. H.; Shiota, Y.; Yoshizawa, K. Methane selective oxidation to methanol by metal-exchanged zeolites: a review of active sites and their reactivity. *Catal. Sci. Technol.* **2019**, *9* (8), 1744−1768.
(27) Ravi, M.; Sushkevich, V. L.; Knorpp, A. J.; Newton, M. A.; Palagin, D.; Pinar, A. B.; Ranocchiari, M.; van Bokhoven, J. A. Misconceptions and challenges in methane-to-methanol over transition-metal-exchanged zeolites. *Nat. Catal.* **2019**, *2* (6), 485−494.
(28) Narsimhan, K.; Iyoki, K.; Dinh, K.; Roman-Leshkov, Y. Catalytic Oxidation of Methane into Methanol over Copper-Exchanged Zeolites with Oxygen at Low Temperature. *ACS Cent. Sci.* **2016**, *2* (6), 424−429.
(29) Xu, J.; Armstrong, R. D.; Shaw, G.; Dummer, N. F.; Freakley, S. J.; Taylor, S. H.; Hutchings, G. J. Continuous selective oxidation of methane to methanol over Cu-and Fe-modified ZSM-5 catalysts in a flow reactor. *Catal. Today* **2016**, *270*, 93−100.
(30) Dinh, K. T.; Sullivan, M. M.; Serna, P.; Meyer, R. J.; Dincă, M.; Román-Leshkov, Y. Viewpoint on the Partial Oxidation of Methane to Methanol Using Cu- and Fe-Exchanged Zeolites. *ACS Catal.* **2018**, *8* (9), 8306−8313.
(31) Latimer, A. A.; Kakekhani, A.; Kulkarni, A. R.; Nørskov, J. K. Direct Methane to Methanol: The Selectivity−Conversion Limit and Design Strategies. *ACS Catal.* **2018**, *8* (6), 6894−6907.
(32) Borfecchia, E.; Beato, P.; Svelle, S.; Olsbye, U.; Lamberti, C.; Bordiga, S. Cu−CHA − a model system for applied selective redox catalysis. *Chem. Soc. Rev.* **2018**, *47* (22), 8097−8133.
(33) Alayon, E. M. C.; Nachtegaal, M.; Bodi, A.; van Bokhoven, J. A. Reaction Conditions of Methane-to-Methanol Conversion Affect the Structure of Active Copper Sites. *ACS Catal.* **2014**, *4* (1), 16−22.
(34) Paolucci, C.; Parekh, A. A.; Khurana, I.; Di Iorio, J. R.; Li, H.; Albarracin Caballero, J. D.; Shih, A. J.; Anggara, T.; Delgass, W. N.; Miller, J. T.; Ribeiro, F. H.; Gounder, R.; Schneider, W. F. Catalysis in a Cage: Condition-Dependent Speciation and Dynamics of Exchanged Cu Cations in SSZ-13 Zeolites. *J. Am. Chem. Soc.* **2016**, *138* (18), 6028−6048.
(35) Di Iorio, J. R.; Gounder, R. Controlling the Isolation and Pairing of Aluminum in Chabazite Zeolites Using Mixtures of Organic and Inorganic Structure-Directing Agents. *Chem. Mater.* **2016**, *28* (7), 2236−2247.
(36) Kulkarni, A. R.; Zhao, Z.-J.; Siahrostami, S.; Nørskov, J. K.; Studt, F. Monocopper Active Site for Partial Methane Oxidation in Cu-Exchanged 8MR Zeolites. *ACS Catal.* **2016**, *6* (10), 6531−6536.
(37) Zhao, Z.-J.; Kulkarni, A.; Vilella, L.; Nørskov, J. K.; Studt, F. Theoretical Insights into the Selective Oxidation of Methane to Methanol in Copper-Exchanged Mordenite. *ACS Catal.* **2016**, *6* (6), 3760−3766.
(38) Doan, H. A.; Li, Z.; Farha, O. K.; Hupp, J. T.; Snurr, R. Q. Theoretical insights into direct methane to methanol conversion over supported dicopper oxo nanoclusters. *Catal. Today* **2018**, *312*, 2−9.
(39) Pappas, D. K.; Borfecchia, E.; Dyballa, M.; Pankin, I. A.; Lomachenko, K. A.; Martini, A.; Signorile, M.; Teketel, S.; Arstad, B.; Berlier, G.; Lamberti, C.; Bordiga, S.; Olsbye, U.; Lillerud, K. P.; Svelle, S.; Beato, P. Methane to Methanol: Structure−Activity Relationships for Cu−CHA. *J. Am. Chem. Soc.* **2017**, *139* (42), 14961−14975.
(40) Mahyuddin, M. H.; Tanaka, T.; Shiota, Y.; Staykov, A.; Yoshizawa, K. Methane Partial Oxidation over $[Cu_2(\mu\text{-}O)]^{2+}$ and $[Cu_3(\mu\text{-}O)_3]^{2+}$ Active Species in Large-Pore Zeolites. *ACS Catal.* **2018**, *8* (2), 1500−1509.

DOI: 10.1021/jacs.9b04906
J. Am. Chem. Soc. 2019, 141, 11641−11650

(41) Alswat, A. A.; Ahmad, M. B.; Hussein, M. Z.; Ibrahim, N. A.; Saleh, T. A. Copper oxide nanoparticles-loaded zeolite and its characteristics and antibacterial activities. *J. Mater. Sci. Technol.* **2017**, *33* (8), 889−896.
(42) Tandon, S. P.; Gupta, J. P. Diffuse Reflectance Spectrum of Cupric Oxide. *Spectrosc. Lett.* **1969**, *2* (12), 357−360.
(43) Gao, F.; Mei, D.; Wang, Y.; Szanyi, J.; Peden, C. H. Selective Catalytic Reduction over Cu/SSZ-13: Linking Homo- and Heterogeneous Catalysis. *J. Am. Chem. Soc.* **2017**, *139* (13), 4935−4942.
(44) Borfecchia, E.; Lomachenko, K. A.; Giordanino, F.; Falsig, H.; Beato, P.; Soldatov, A. V.; Bordiga, S.; Lamberti, C. Revisiting the nature of Cu sites in the activated Cu-SSZ-13 catalyst for SCR reaction. *Chem. Sci.* **2015**, *6* (1), 548−563.
(45) Gao, F.; Kwak, J. H.; Szanyi, J.; Peden, C. H. F. Current Understanding of Cu-Exchanged Chabazite Molecular Sieves for Use as Commercial Diesel Engine DeNOx Catalysts. *Top. Catal.* **2013**, *56* (15−17), 1441−1459.
(46) Paolucci, C.; Khurana, I.; Parekh, A. A.; Li, S.; Shih, A. J.; Li, H.; Di Iorio, J. R.; Albarracin-Caballero, J. D.; Yezerets, A.; Miller, J. T.; Delgass, W. N.; Ribeiro, F. H.; Schneider, W. F.; Gounder, R. Dynamic multinuclear sites formed by mobilized copper ions in NOx selective catalytic reduction. *Science* **2017**, *357* (6354), 898−903.
(47) Paolucci, C.; Verma, A. A.; Bates, S. A.; Kispersky, V. F.; Miller, J. T.; Gounder, R.; Delgass, W. N.; Ribeiro, F. H.; Schneider, W. F. Isolation of the copper redox steps in the standard selective catalytic reduction on Cu-SSZ-13. *Angew. Chem., Int. Ed.* **2014**, *53* (44), 11828−11833.
(48) Di Iorio, J. R.; Bates, S. A.; Verma, A. A.; Delgass, W. N.; Ribeiro, F. H.; Miller, J. T.; Gounder, R. The Dynamic Nature of Brønsted Acid Sites in Cu−Zeolites During NOx Selective Catalytic Reduction: Quantification by Gas-Phase Ammonia Titration. *Top. Catal.* **2015**, *58* (7−9), 424−434.
(49) Moreno-González, M.; Hueso, B.; Boronat, M.; Blasco, T.; Corma, A. Ammonia-containing species formed in Cu-chabazite as per in situ EPR, solid-state NMR, and DFT calculations. *J. Phys. Chem. Lett.* **2015**, *6* (6), 1011−1017.
(50) Szanyi, J.; Kwak, J. H.; Zhu, H.; Peden, C. H. Characterization of Cu-SSZ-13 NH_3 SCR catalysts: an in situ FTIR study. *Phys. Chem. Chem. Phys.* **2013**, *15* (7), 2368−2380.
(51) Bordiga, S.; Groppo, E.; Agostini, G.; van Bokhoven, J. A.; Lamberti, C. Reactivity of Surface Species in Heterogeneous Catalysts Probed by In Situ X-ray Absorption Techniques. *Chem. Rev.* **2013**, *113* (3), 1736−1850.
(52) Li, H.; Paolucci, C.; Khurana, I.; Wilcox, L. N.; Goltl, F.; Albarracin-Caballero, J. D.; Shih, A. J.; Ribeiro, F. H.; Gounder, R.; Schneider, W. F. Consequences of exchange-site heterogeneity and dynamics on the UV-visible spectrum of Cu-exchanged SSZ-13. *Chem. Sci.* **2019**, *10* (8), 2373−2384.
(53) Li, H.; Paolucci, C.; Khurana, I.; Wilcox, L. N.; Göltl, F.; Albarracin-Caballero, J. D.; Shih, A. J.; Ribeiro, F. H.; Gounder, R.; Schneider, W. F. Consequences of exchange-site heterogeneity and dynamics on the UV-visible spectrum of Cu-exchanged SSZ-13. *Chem. Sci.* **2019**, *10* (8), 2373−2384.
(54) Psofogiannakis, G. M.; McCleerey, J. F.; Jaramillo, E.; van Duin, A. C. T. ReaxFF Reactive Molecular Dynamics Simulation of the Hydration of Cu-SSZ-13 Zeolite and the Formation of Cu Dimers. *J. Phys. Chem. C* **2015**, *119* (12), 6678−6686.
(55) Göltl, F.; Love, A. M.; Hermans, I. Developing a Thermodynamic Model for the Interactions between Water and Cu in the Zeolite SSZ-13. *J. Phys. Chem. C* **2017**, *121* (11), 6160−6169.
(56) Perea, D. E.; Arslan, I.; Liu, J.; Ristanović, Z.; Kovarik, L.; Arey, B. W.; Lercher, J. A.; Bare, S. R.; Weckhuysen, B. M. Determining the location and nearest neighbours of aluminium in zeolites with atom probe tomography. *Nat. Commun.* **2015**, *6*, 7589−7597.
(57) Han, O. H.; Kim, C.-S.; Hong, S. B. Direct Evidence for the Nonrandom Nature of Al Substitution in Zeolite ZSM-5: An Investigation by 27Al MAS and MQ MAS NMR. *Angew. Chem., Int. Ed.* **2002**, *41* (3), 469−472.

DOI: 10.1021/jacs.9b04906
J. Am. Chem. Soc. 2019, 141, 11641−11650